Performance Comparison Between Spatial Multiplexing and Spatial Modulation in Indoor MIMO Visible Light Communication Systems

Cuiwei He, Thomas Q. Wang, and Jean Armstrong
Department of Electrical and Computer Systems Engineering,
Monash University,
Melbourne, Australia
{Cuiwei.He, Tom.Wang, Jean.Armstrong}@monash.edu

***Abstract*—Spatial multiplexing (SMP) and optical spatial modulation (OSM) are two important technologies for indoor multiple-input multiple-output (MIMO) visible light communications (VLC). In this paper, we compare the performance of SMP and OSM systems which are operated with typical configurations in an indoor scenario. Both systems transmit data using asymmetrically clipped optical orthogonal frequency division multiplexing (ACO-OFDM) as the modulation scheme. It is shown that in order to achieve the same data rate with the SMP, the OSM has to employ large constellations which become impractical when either the number of luminaires or the constellation size of the SMP is greater than four. Simulation results are presented for both MIMO systems using four luminaires as transmitters and a receiver configured with three different front-ends. These receivers include a conventional non-imaging receiver, a prism-based receiver and an aperture-based receiver. The BER results demonstrate that SMP outperforms OSM in terms of both the size of the region in which a receiver can achieve low BER and the BER at typical receiver positions.**

Keywords— spatial multiplexing (SMP), optical spatial modulation (OSM), visible light communications (VLC), asymmetrically clipped optical orthogonal frequency division multiplexing (ACO-OFDM), zero-forcing (ZF), multiple-input multiple-output (MIMO)

I. INTRODUCTION

With the increasing implementation of light emitting diodes (LEDs), indoor visible light communication (VLC) is emerging as a promising dual-use technology for both lighting and data transmission [1]. The illumination in modern indoor scenarios is typically provided by LED luminaires installed at intervals in the ceiling. This is stimulating the development of a range of novel multiple-input multiple-output (MIMO) VLC systems that use ceiling lights to transmit data streams and multiple receiving elements (REs) for de-multiplexing and decoding [2-6].

The luminaires used as transmitters in a MIMO VLC system can be configured in a number of ways. The most straightforward way is spatial multiplexing (SMP) in which the luminaires emit independent data streams. This potentially provides the highest data rate that an indoor VLC system can achieve [2, 7]. As multiple data streams are received simultaneously, the received signals are typically subject to strong multi-stream interference (MSI). Alternatively, optical spatial modulation (OSM) can be applied, in which the information is conveyed by both the data symbols modulated on the light intensity and the index of the active luminaire [4, 8]. As the data symbols are transmitted orthogonally in the frequency domain by different luminaires, MSI is absent [8]. However, this avoidance of the MSI is achieved at the cost of a significant reduction in data rate. A comparison of bit error rates (BERs) between the SMP and the OSM using imaging receivers is presented in [9]. However, this comparison assumes good alignments between the transceivers which, in practice, may have different relative positions.

In both SMP MIMO and OSM MIMO systems, it is crucial for the receiver to decouple multiple transmitted signals [9]. This means that well-conditioned channel matrices are desirable for both MIMO systems. Recent studies have reported a range of designs for the receiver front-end, including prism-array receivers [6], aperture-based receivers [7], and *K*-FOV receivers [10] and shown that these receivers can lead to well-conditioned channel matrices.

In this paper, we compare the bit error rate (BER) performance of the SMP and the OSM systems in a typical indoor scenario. The two MIMO systems are studied with a range of receiver front-ends including a conventional non-imaging receiver (1-FOV receiver) [10], a prism-array receiver [6] and an aperture-based receiver [7]. In order to avoid unfair comparisons, zero-forcing (ZF) equalizers are used in the receivers for both the SMP and OSM to decouple the signals transmitted by different luminaires. We present simulation results for systems using asymmetrically clipped optical orthogonal frequency division multiplexing (ACO-OFDM) as the modulation scheme. ACO-OFDM is currently attracting widespread interest because it has the flexibility of a multicarrier system while also being very power efficient for small and medium sizes of constellations [11]. We show that, in order to achieve the same data rate with SMP, OSM has to employ large constellations which become impractical when either the number of luminaires or the constellation size of the SMP is greater than four. The simulation results show that SMP outperforms OSM in terms of both the size of the region in which a receiver can achieve low BER and the BER at typical receiver positions.

This work was supported under Australian Research Council's (ARC) Discovery funding schemes (DP 130101265) and (DP 150100003).

II. INDOOR MIMO VLC SYSTEMS

Fig. 1 shows a typical VLC system in an indoor scenario with dimensions of X m$\times Y$ m$\times Z$ m. N_{t} LED luminaires are installed on the ceiling, pointing directly downwards to illuminate the room and to transmit information. A MIMO receiver is placed at a height of T m above the floor, facing upwards, where T is typically the height of a table. The receiver consists of N_{r}, $N_{\mathrm{r}} \geq N_{\mathrm{t}}$, receiving elements (REs) which convert the received optical signals to photocurrents for decoding. We consider three different configurations for the front-end of the receiver: a) the 1-FOV receiver which consists of N_{r} PDs [10]; b) the aperture-based receiver in which each RE comprises an aperture and a bare PD [7]; c) the prism-array based receiver in which each RE consists of a prism and a PD [6]. Thus, the VLC channels between the luminaires and the receiver can be denoted by an $N_{\mathrm{r}} \times N_{\mathrm{t}}$ matrix, $\mathbf{H}$, with the element $\mathbf{H}(i,j)$ representing the channel gain between the jth luminaire and ith RE.

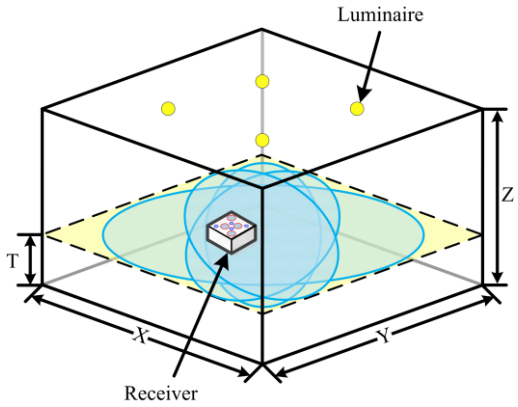

Fig. 1. Indoor visible light communication configuration

In this paper, the MIMO VLC is configured to transmit ACO-OFDM signals using either SMP or OSM. SMP employs all the luminaires to emit independent streams which have all the odd subcarriers loaded with data symbols [6]. For OSM, however, the information is conveyed through both the data symbol on the odd subcarrier and the index of the luminaire which transmits the symbol on that subcarrier [8].

A. SMP MIMO System

The SMP MIMO system studied in this paper transmits N_{t} independent data streams modulated using ACO-OFDM. Each transmitter comprises an ACO-OFDM modulator which converts the complex bipolar data symbols $\mathbf{X}^{(j)} = \left[0, X_1^{(j)}, 0, X_3^{(j)}, \ldots, X_{N-1}^{(j)}\right]$, $j = 1, 2, \ldots, N_{\mathrm{t}}$ to real nonnegative signals $s_{\mathrm{ACO,\,SMP}}^{(j)}(t)$, and a LED luminaire that modulates the signals onto light intensity. Here the superscript and the subscript of each data symbol denote the index of the luminaire and the index of the subcarrier, respectively. We assume that signal $s_{\mathrm{ACO,\,SMP}}^{(j)}(t)$, $j = 1, \ldots, N_{\mathrm{t}}$, has a bandwidth smaller than the modulation bandwidth of the LED, so that the luminaires do not distort the signal waveform. We further assume, without loss of generality, unit conversion factor from the electrical domain to the optical domain in the luminaires.

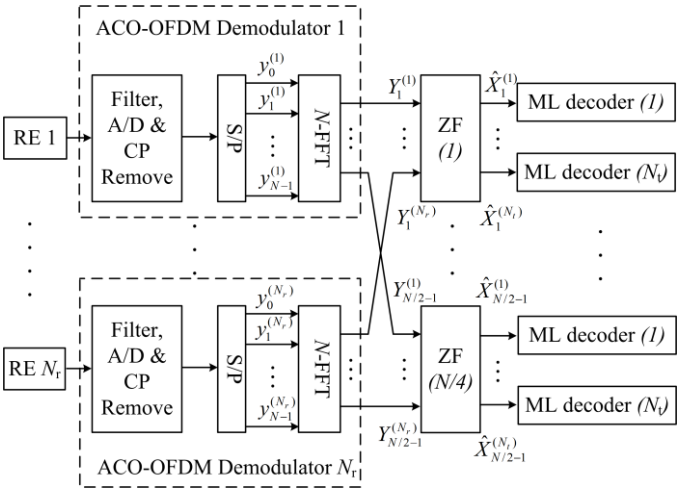

Fig. 2. The strucure of the SMP MIMO receiver

It can be shown that as long as the number of independently modulated subcarriers is large enough, the ACO-OFDM signal has a truncated Gaussian distribution with optical power, $P_{\mathrm{opt,\,SMP}}$, given by [12]

$$P_{\mathrm{opt,\,SMP}} = E\left(s_{\mathrm{ACO,\,SMP}}^{(j)}(t)\right) = \sigma_{\mathrm{x}} / \sqrt{2\pi}, \qquad (1)$$

where σ_{x} is given by $\sigma_{\mathrm{x}} = \left(E_{\mathrm{x}}/2\right)^{1/2}$, where $E_{\mathrm{x}} = E\left(\left|X_k^{(j)}\right|^2\right)$. Therefore, the average transmitted optical energy per bit, $E_{\mathrm{b,opt,\,SMP}}$, can be expressed as $E_{\mathrm{b,opt,\,SMP}} = P_{\mathrm{opt,\,SMP}} / b_{\mathrm{SMP}}$, where b_{SMP} denotes the bit rate of the ACO-OFDM signal emitted by each luminaire.

The receiver of the SMP system is shown in Fig. 2. As shown in the figure, each RE is connected to an ACO-OFDM demodulator which converts the received signals from the time domain to the frequency domain. Then, the signals on a given subcarrier are sent into the corresponding de-multiplexing device which is a zero-forcing (ZF) equalizer, followed by the maximum likelihood (ML) decoders.

B. OSM MIMO System

Fig. 3 shows the OSM system using ACO-OFDM. As shown in the figure, the OSM system conveys information using both the data symbol modulated onto the light intensity and the index of the active LED. As the data symbols are modulated using ACO-OFDM, they are loaded only onto the odd subcarriers and have Hermitian symmetry at the inputs of the IFFTs in the transmitters [13]. The original OSM encoding [4] is applied on the odd subcarriers, assigning the subgroups of subcarriers to different transmitters in accordance with the extra data symbols that are mapped to the index of the luminaires [8]. Note that because of the Hermitian symmetry, the kth and the $(N-k)$th subcarriers must be assigned to the

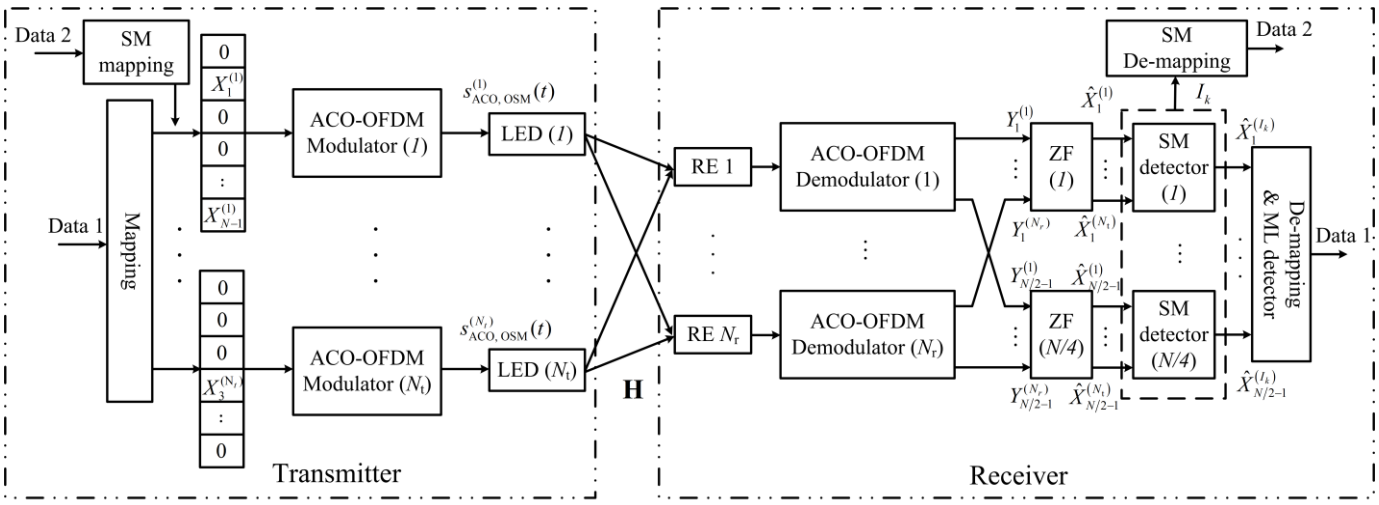

Fig. 3. Structure of an OSM ACO-OFDM system

same luminaire. This means that the extra symbols can only provide $N\log_2(N_t)/4$ bits other than $N\log_2(N_t)$ bits as its RF counterpart.

Assuming that the extra symbols are independent and have equal probability, the number of the subcarriers assigned to each luminaire is approximately $N/(2N_t)$ when the number of subcarriers is large enough. Then, the optical power, $P_{\text{opt,OSM}}$, and the optical energy per bit, $E_{\text{b, opt, OSM}}$ can be expressed as

$$\begin{aligned} P_{\text{opt,OSM}} &= E\left(s^{(j)}_{\text{ACO, OSM}}\right) = \sigma_x \Big/ \left(\sqrt{2\pi N_t}\right), \\ E_{\text{b, opt, OSM}} &= P_{\text{opt,OSM}} / b_{\text{OSM}} \end{aligned} \tag{2}$$

respectively, where b_{OSM} denotes the average bit rate per luminaire.

The signal processing modules of the OSM receiver are identical to those of the SMP receiver apart from the SM detectors and the ML decoders at the outputs of the ZF equalizers. The SM detectors decode the information carried by the extra symbols and return the index of the active luminaire, given by

$$I_k = \arg\max_j \left(\left|\hat{X}^{(j)}_{k,\text{sm}}\right|\right), j = 1,\ldots,N_t,\ k = 1,3,\ldots,N/2-1 \ , \tag{3}$$

where $\hat{X}^{(j)}_{k,\text{sm}}$ denotes the jth output of the ZF equalizer decoupling signals on the kth subcarrier. Only the output, $\hat{X}^{(I_k)}_{k,\text{sm}}$, is then sent into the ML decoder to recover the data symbol on the kth subcarrier.

III. Comparisons between SMP MIMO and OSM MIMO

A. Configurations for the simulations

In this section, we compare the BER performance of the SMP and OSM systems using receivers with different front-end configurations. We consider a room, shown in Fig. 1, with dimensions of $3\text{ m}\times 3\text{ m}\times 2.5\text{ m}$. Fig. 5 shows the top-view of the room and the associated coordinate system, $\hat{x}\hat{O}\hat{y}$. Four Lambertian LED luminaires with semi-angle of 60° at half power are mounted on the ceiling with coordinates: LED1 $(0.6, 2.4)$, LED2 $(2.4, 2.4)$, LED3 $(0.6, 0.6)$ and LED4 $(2.4, 0.6)$, respectively. All the LEDs have identical transmitted optical power of three Watts, i.e. $P_{\text{opt}} = P_{\text{opt, OSM}} = P_{\text{opt, SMP}} = 3\text{ W}$. The data symbols are modulated using ACO-OFDM with $N = 256$ subcarriers and a bandwidth of 2 MHz, which is limited by the modulation bandwidth of the white LEDs [14].

TABLE I. Specifications for the receivers

	Non-imaging receiver [10]	Prism-based receiver [6]	Aperture-based receiver [7]
Light collecting area per RE	π mm^2	π mm^2	π mm^2
Number of REs	8	8	8
Spacing between the REs	$S_1 = 3$ cm $S_2 = 1.5$ cm	N/A	N/A
β angle	N/A	30°	N/A
Index of refraction of prisms	N/A	1.5	N/A
Radial distance between aperture and PD	N/A	N/A	1.5 mm
Polar angle of the PD relative to aperture	N/A	N/A	$\frac{\pi}{4}j, j = 1,\ldots,8$

A receiver with eight REs is placed 0.8 m above the floor. The key parameters for the receivers are listed in Table I. Note that the light collecting area shown in Table I is given by the

effective area of the PD for the conventional non-imaging receiver, the area of the top surface of each prism for the prism-array receiver and the area of the aperture and that of the PD for the aperture-based receiver.

The received signals, in general, consist of two components: the line of sight (LOS) component and the diffuse component. Previous studies have shown that the LOS component is typically stronger than the diffuse component [2]. Therefore, in line with other papers [2, 3], we consider only the LOS component and the channel gains can be calculated as shown in [6, 7, 10]. Consequently, the frequency response of the optical channel is flat with the same channel matrices for all the subcarriers, resulting in identical ZF equalizers for each subcarrier.

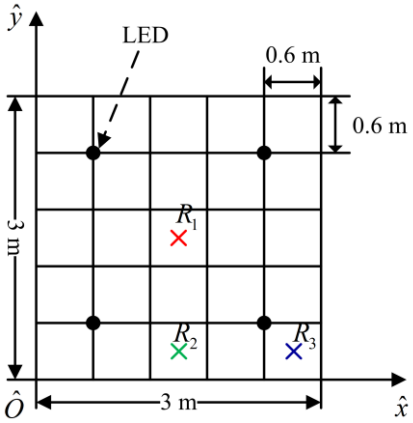

Fig. 4. Top-view of the room

We consider shot noise only. This results from the ambient light and can be modeled as a white Gaussian process with single-sided power density given by [15]

$$N_0 = 2qR_{\mathrm{p}}p_{\mathrm{n}}A\Delta\lambda \ , \tag{4}$$

where q is the electron charge, p_{n} is the background spectral irradiance, A is the light collecting area of the RE and $\Delta\lambda$ is the bandwidth of the light spectrum. Note that as the prism-array receiver and the aperture-based receiver employ directional REs, the power density given by (4) is only an estimate for these receivers. The real value will be smaller because some ambient light is blocked by the opaque coating for aperture-based receivers and that some is reflected away by the prism surfaces for prism-array receivers. In this paper, we assume the responsivity of the PDs is 0.4 A/W in line with [2]. The bandwidth in (4), $\Delta\lambda$, is 300 nm which is approximately the bandwidth of visible light.

In order to avoid unfair comparisons, we assume the two systems transmit information at the same data rate, i.e. $b_{\mathrm{SMP}} = b_{\mathrm{OSM}} = b$ and thus $E_{\mathrm{b,\,opt,\,SMP}} = E_{\mathrm{b,\,opt,\,OSM}} = E_{\mathrm{b,\,opt}}$. The numbers of bits transmitted per MIMO OFDM symbol for the SMP and OSM are given by $\left(N_{\mathrm{t}}N\log_2 M_{\mathrm{SMP}}\right)/4$ and $\left(N\log_2\left(N_{\mathrm{t}}M_{\mathrm{OSM}}\right)\right)/4$, respectively. Therefore, assuming that the two systems have the same OFDM block duration, the number of bits transmitted for both MIMO systems must be the same, i.e.

$$\left(M_{\mathrm{SMP}}\right)^{N_{\mathrm{t}}} = N_{\mathrm{t}}M_{\mathrm{OSM}} \ . \tag{5}$$

From (5), we can see that the size of the constellation for SM MIMO will be impractically large when either the size of the constellation, M_{SMP} , or the number of the luminaire is greater than four. Thus, in this paper, the sizes of the constellation, M_{SMP} and M_{OSM} are given by 4 and 64, respectively.

B. Simulation Results

1) BER distributions as a function of the receiver position

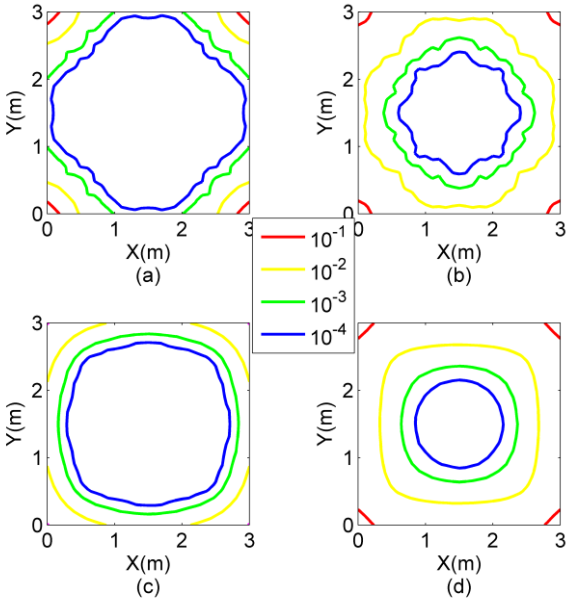

Fig. 5. Contour plot of BER distribution with $E_{\mathrm{b,opt}}/N_0$ at 163 dB using (a) prism-array receiver in the SMP MIMO system (b) prism-array receiver in the OSM MIMO system (c) aperture-based receiver in the SMP MIMO system (d) aperture-based receiver in the OSM MIMO system.

We first study the BER distributions with the prism-array receiver and the aperture-based receiver. The rank of the channel matrices was examined at all possible receiver positions for both of the receivers. The results show that the channel matrices have full rank at all possible receiver positions. This indicates that the transmitted signals can be separated at the receiver using ZF equalizers. Fig. 5 shows the contours of the BER as a function of the receiver position, $\hat{x}\hat{O}\hat{y}$, shown in Fig. 4, with the value of $E_{\mathrm{b,opt}}/N_0$ at 163 dB. Using (4), this corresponds to a background spectral irradiance of 1.25×10^{-4} $\mathrm{W}/\left(\mathrm{nm}\cdot\mathrm{cm}^2\right)$ which is greater than the worst case in the daytime near the window [16]. Thus this figure shows the BER with intense ambient light and the BER will be much lower in a real indoor scenario. As shown in the figure, the contours present as co-centered rings, with low BER located in the central area and large BER near the walls and the corners. The size of the low BER region in which the BER $<10^{-3}$, depends on both the configuration of the

receiver front-end and the transmission scheme. From this figure, we can see that the SMP with the prism-array receiver achieves the largest low BER region followed by the SMP with the aperture-based receiver. This means that both of the receivers can provide good performance when SMP is applied. As neither of the receivers is optimized for the considered indoor scenario, general conclusions that prism-array receivers always outperform aperture-based receivers cannot be made. The OSM MIMO, however, results in small low BER regions which only cover the central area of the room as shown in Fig. 5(b) and (d). This is mainly caused by the use of a relatively large constellation size. Consequently, we can see that the SMP outperforms OSM in term of the size of the region in which low BER is achieved.

2) BER performance at typical receiver positions

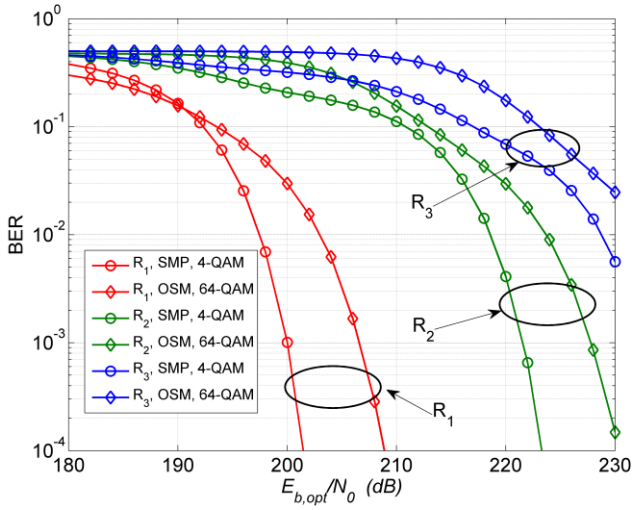

Fig. 6. BER versus $E_{\mathrm{b,opt}}/N_0$ (dB) at three specific receiver positions using conventional non-imaging receiver

Now we compare the BER achieved by SMP and OSM at typical receiver positions: $R_1(1.5,1.5)$, $R_2(1.5,0.3)$ and $R_3(2.7,0.3)$ where R_1 is located at the center of the room, R_2 near the wall, and R_3 near the corner. The results are shown in Fig. 6-8 for the non-imaging receiver, the prism-array receiver and the aperture-based receiver, respectively. Note that as the non-imaging receiver normally results in ill-conditioned channel matrices, the scale for $E_{\mathrm{b,opt}}/N_0$ in Fig. 6 ranges from 180 dB to 230 dB which is much higher than those in Fig. 7 and 8. From these figures, we can see that the SMP outperforms the OSM at all three receiver positions for all three receiver front-ends. This is because the decoding of OSM signals are typically subject to two adverse facts. First, the decoding is performed in two successive procedures: the de-mapping of the active luminaire and the ML decoding. An error in either procedure can result in a failure of the decoding. Secondly, the large constellation used to achieve identical data rate with SMP leads to high BERs at low values for $E_{\mathrm{b,opt}}/N_0$. Therefore, we can see a gap of the BER between the SMP and the OSM, which is independent of the type of the receiver front-end that is used and of the receiver position. For example, a 7 dB difference is observed at the BER of 10^{-4} for all the type of receivers at all the receiver positions.

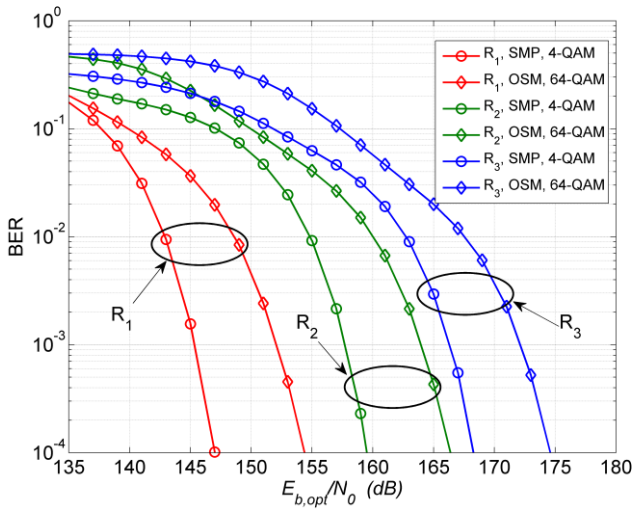

Fig. 7. BER versus $E_{\mathrm{b,opt}}/N_0$ (dB) at three specific receiver positions using prism-array receiver

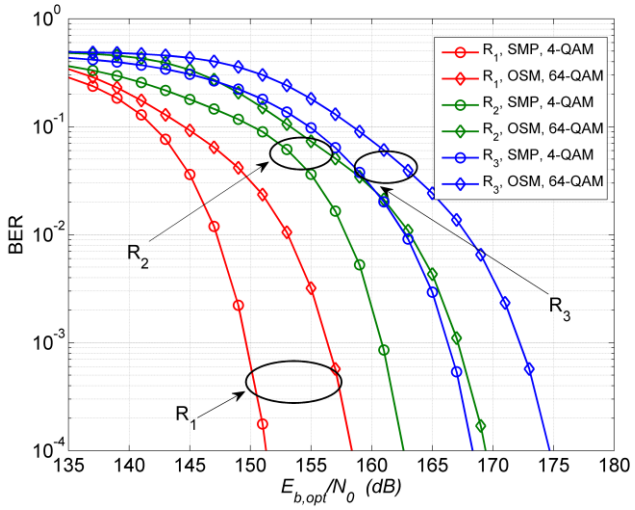

Fig. 8. BER versus $E_{\mathrm{b,opt}}/N_0$ (dB) at three specific receiver positions using aperture-based receiver

Fig. 9 shows the BER versus $E_{\mathrm{b,opt}}/N_0$ for the SMP MIMO and the OSM MIMO systems when both are using 64-QAM symbols. Note that this means the overall data rate for OSM is much lower than for SMP as can be seen from (5). Here the prism-array receiver and the aperture-based receiver are at receiver position, R_1. From this figure, we can see that OSM has a lower BER than SMP at low $E_{\mathrm{b,opt}}/N_0$ values, but the BER curves converge at high values. This is because the overall BER in the OSM system has a number of components. The BER values for these different components reduce at different rates as $E_{\mathrm{b,opt}}/N_0$ increases. The probability of the SM decoder returning an error for I_k depends on the

value $|X_k|^2$ as well as the ratio $E\{|X_k|^2\}/E\{|N_k|^2\}$, where N_k is the noise component on the kth subcarrier. This is because I_k is incorrectly decoded if the power of the noise alone is greater for an incorrect index is greater than the power of the signal plus noise on the correct index. This is much more likely for constellation points with small $|X_k|$. So most errors in decoding the index will be from subcarriers modulated by inner constellation points. Rather surprisingly, in this case, an error in decoding the index does not mean that there will be a large number of errors in decoding the constellation. This is because the noise alone on the incorrectly decoded index is unlikely to be very large so is likely to be demapped to an inner constellation point. Assuming Gray coded data, at a high possibility, the four bits of the 64-QAM data will still be correctly decoded. At all signal-to-noise ratios (SNRs), this form of error event is more likely than errors in decoding the QAM constellation alone. It reduces more slowly with increasing SNR than the constellation errors in the SMP system so the results converge at higher $E_{\mathrm{b,opt}}/N_0$. So at high $E_{\mathrm{b,opt}}/N_0$ the OSM has similar BER to SMP and has a significantly lower data rate.

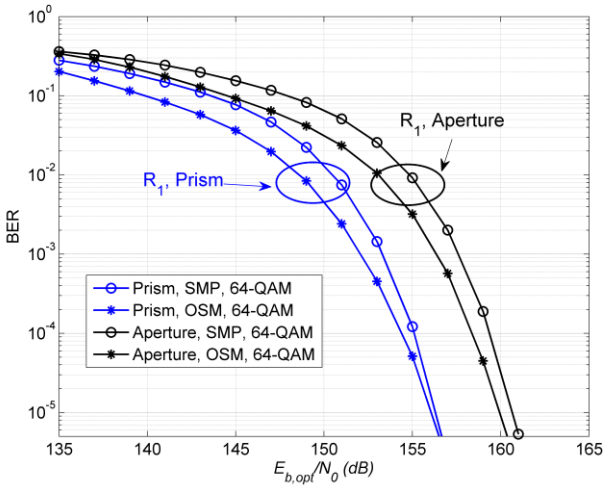

Fig. 9. BER versus $E_{\mathrm{b,opt}}/N_0$ (dB) at R_1 using prism-array and aperture-based receivers

IV. Conclusion

In this paper, we have compared the BER performance of SMP and OSM systems operated with typical parameters in indoor MIMO optical wireless communications. The two MIMO systems are studied with a range of configurations for the receiver front-end, including a conventional non-imaging receiver, a prism-array receiver and an aperture-based receiver. We show that in order to achieve the same data rate with the SMP, the OSM has to use impractically large constellations when either the number of luminaires or the constellation size of SMP is greater than four. Simulation results are presented for the case where the SMP transmits 4-QAM symbols and the OSM, 64-QAM symbols using four luminaires in a typical room. The distribution of the BERs as a function of the receiver position are compared between the two MIMO systems, demonstrating that the SMP can achieve much greater LBR whereas the LBR for the OSM covers only the central area of the room. The BER results also show that the SMP outperforms at typical receiver positions when the two MIMO systems transmit data at identical rate. A constant gap of 7 dB between the two MIMO systems is observed at the BER of 10^{-4} irrespective of the type of the receiver front-end.

References

[1] M. Rahaim, M. Hella, A. Mirvakilli, S. Ray, V. J. Koomson, and T. D. C. Little, "Software Defined Visible Light Communication," in *Wireless Innovation Forum Conference on Communications Technologies and Software Defined Radio (SDR-WinnComm 2014)*, Schaumburg, Illinois, 2014.

[2] L. Zeng, D. O'Brien, H. L. Minh, G. Faulkner, K. Lee, D. Jung, et al., "High data rate multiple input multiple output (MIMO) optical wireless communications using white led lighting," *IEEE J. Sel. Areas Commun.*, vol. 27, pp. 1654-1662, 2009.

[3] T. Fath and H. Haas, "Performance Comparison of MIMO Techniques for Optical Wireless Communications in Indoor Environments," *IEEE Trans. Commun.*, vol. 61, pp. 733-742, Feb. 2013.

[4] R. Mesleh, H. Elgala, and H. Haas, "Optical Spatial Modulation," *IEEE/OSA J. Opt. Commun. Netw.*, vol. 3, pp. 234-244, March 2011.

[5] T. Q. Wang, Y. A. Sekercioglu, and J. Armstrong, "Analysis of an Optical Wireless Receiver Using a Hemispherical Lens With Application in MIMO Visible Light Communications," *IEEE/OSA J. Lightw. Technol.*, vol. 31, pp. 1744-1754, June 2013.

[6] T. Q. Wang, R. J. Green, and J. Armstrong, "MIMO Optical Wireless Communications using ACO-OFDM and a Prism-Array Receiver," *IEEE J. Sel. Areas Commun.*, vol. 33, pp. 1959-1971, Sep. 2015.

[7] T. Q. Wang, C. He, and J. Armstrong, "Angular Diversity for Indoor MIMO Optical Wireless Communications," in *Int. Conf. on Communications*, London, 2015, pp. 5066-5071.

[8] Y. Li, D. Tsonev, and H. Haas, "Non-DC-Biased OFDM with Optical Spatial Modulation," in *International Symposium on Personal Indoor and Mobile Radio Communications (PIMRC)*, London, 2013, pp. 486-490.

[9] P. M. Butala, H. Elgala, and T. D. C. Little, "Performance of optical spatial modulation and spatial multiplexing with imaging receiver," in *IEEE Wireless Communications and Networking Conference (WCNC)*, Istanbul, 2014, pp. 394-399.

[10] C. He, T. Q. Wang, and J. Armstrong, "Performance of Optical Receiver Using Photodetectors with Different Fields of View in a MIMO ACO-OFDM System," *IEEE/OSA J. Lightw. Technol.*, vol. 33, pp. 4957-4967, 2015.

[11] J. Armstrong and B. J. C. Schmidt, "Comparison of asymmetrically clipped optical OFDM and DC-biased optical OFDM in AWGN," *IEEE Commun. Lett.*, vol. 12, pp. 343-345, May 2008.

[12] S. D. Dissanayake and J. Armstrong, "Comparison of ACO-OFDM, DCO-OFDM and ADO-OFDM in IM/DD Systems," *IEEE/OSA J. Lightw. Technol.*, vol. 31, pp. 1063-1072, Apr. 2013.

[13] J. Armstrong and A. J. Lowery, "Power efficient optical OFDM," *Electron. Lett.*, vol. 42, pp. 370-2, 2006.

[14] J. Grubor, S. Randel, K. D. Langer, and J. W. Walewski, "Broadband information broadcasting using LED-based interior lighting," *IEEE/OSA J. Lightw. Technol.*, vol. 26, pp. 3883-3892, Dec. 2008.

[15] J. M. Kahn and J. R. Barry, "Wireless infrared communications," *Proc. IEEE*, vol. 85, pp. 265-298, 1997.

[16] J. R. Barry, *Wireless Infrared Communications*. New York: Kluwer Academic Publishers, 1994.